Pergamon

Int. J. Solids Structures Vol. 35, No. 21, pp. 2749–2773, 1998

0020-7683/98 $19.00 + .00

PII: S0020-7683(97)00240-0

BONDED REPAIR OF CRACKS UNDER MIXED MODE LOADING

C. H. WANG and L. R. F. ROSE
Aeronautical and Maritime Research Laboratory, Defence Science and Technology Organisation, 506 Lorimer Street, Fishermens Bend, Melbourne, 3207, Australia

(*Received* 22 *December* 1996; *in revised form* 24 *July* 1997)

Abstract—The problem of assessing the effectiveness of a bonded repair to a cracked plate can be reduced to a one-dimensional integral equation for the special case when both the plate and the reinforcement are isotropic and have the same Poisson's ratio. This special case is used here to highlight some aspects of bonded repair efficiency under mixed mode loading which are not captured by crack bridging models. It is shown that bonded repair is less efficient in reducing the stress intensity factor under mode II than mode I, although the stress intensity factor under the shear mode also asymptotes to a limiting value as has been previously shown for the tensile mode. A closed form solution is derived for the limiting value of the stress intensity factor under shear mode. It is shown that for the long crack limit, the appropriate two-dimensional idealisation of the representative bonded joint corresponds to a plane strain condition, and the existing asymptotic solution for tensile mode needs to be modified to accommodate the effect of Poisson's ratio on the stress intensity factor. It is also noted that crack bridging models lead to non-conservative predictions of repair efficiency for short cracks.

1. INTRODUCTION

In the last two decades bonded repair technology has proved a cost-effective means of repairing cracks in aircraft structures (Ratwani, 1979; Rose, 1981; Baker and Jones, 1988; Baker, 1993; Baker, 1995; Rose *et al.*, 1995). The simple fact that the stress intensity factor of a crack after repair asymptotes to a limiting value as the crack length increases plays a key role in successful applications of this technique. However, analyses so far have been limited to the tensile mode only and it is not clear whether bonded repair is equally effective in reducing the stress intensity factor of a crack subjected to shear loading, or mixed mode loading in general.

Although cracks that are likely to be encountered in practice are generally aligned in a direction perpendicular to the principal tensile stress (or strain), giving rise to mode I cracking, there are at least two circumstances where mixed mode cracking is a major concern in the context of bonded repair. Firstly, application of bonded reinforcements, which are frequently anisotropic, may alter the local stress state near the crack region so that the maximum principal stress may no longer remain perpendicular to the crack plane. Secondly, structures are frequently subjected to non-proportional loading in which the principal stress/strain axes rotate with time (see e.g. Wang and Brown, 1993, 1996), thus cracks may experience a time-dependent mixed mode loading. If the bonded repair technique is used to repair mode II cracks, one important question remaining to be resolved is whether this method is still effective. In particular, one recent finite element study by Chue *et al.* (1994) showed that the repair efficiency for mode II cracks was much lower than for mode I.

A typical bonded repair consists of two sheets which are bonded together by a thin layer of adhesive; see, e.g. Fig. 1. Since a bonded repair represents a multiple layered structure with a crack being present in only one layer, an exact, analytical solution of this three-dimensional problem is an almost intractable task. Hence it is imperative to make simplifications of some sort to enable the problem to be analysed. Three approaches have been proposed so far to simplify the problem of bonded repairs to either a one-dimensional or two-dimensional problem. By idealising the adhesive layer as shear springs and treating the stresses in the adhesive layer as body forces acting on the mid-plane of the plate and

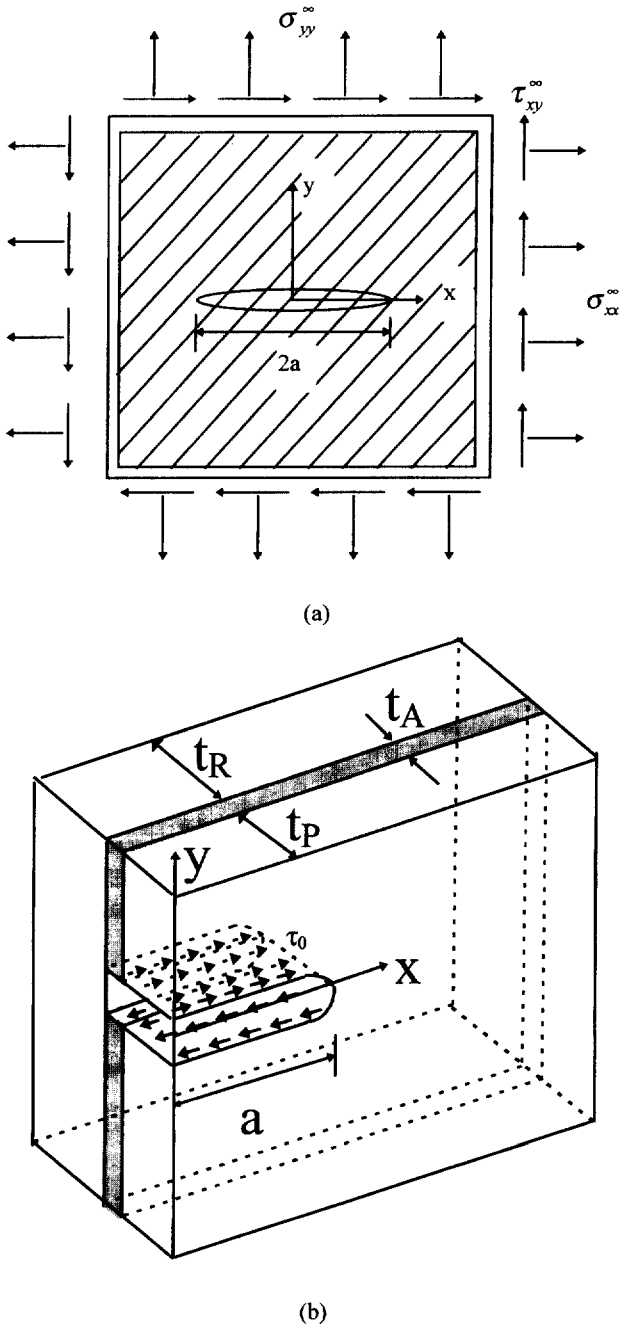

Fig. 1. A centre cracked plate repaired by a bonded patch and subjected to mixed mode loading. (a) Plan view and (b) near crack region for the perturbation shear loading case.

the reinforcement, Erdogan and Arin (1972) modelled a bonded repair as a two-dimensional structure subjected to in-plane loading, making use of the solution of a centre-cracked sheet subjected to a point force at arbitrary position. One set of coupled 2-D integral equations was obtained for the two shear stresses in the adhesive layer. Based on similar assumptions, Keer *et al.* (1976) proposed an elegant approach for the special case of an isotropic plate and reinforcement having identical Poisson's ratio. Under this condition, the problem was successfully reduced to a single 1-D integral equation, with the integral ranging over the crack length. Compared with the method by Erdogan and Arin (1972), Keer's formulation is considerably more efficient for parametric studies of the various factors affecting repair efficiency.

An alternative, simpler method for modelling crack patching would be to model the bonded repair as cracks bridged by springs, resulting in essentially a one-dimensional equilibrium problem (Rose, 1987; Budiansky *et al.*, 1988). The crack bridging model involves two separate steps. Firstly an appropriate spring constant is determined, for example from an overlap bonded joint (Rose, 1982) representing the central strip of a bonded repair. Then the bonded repair was modelled as a crack internally reinforced by springs. Although this crack bridging model is now well established for dealing with bonded repairs and fibre bridging in composite materials (Nemat-Nasser and Hori, 1987), this one-dimensional idealisation is inadequate in the short crack limit, mainly because it does not account for the in-plane shear transfer between neighbouring strips parallel to the load axis. Thus, the asymptotic expansion of the stress intensity factor determined from the spring model in the short crack limit (Rose, 1987) differed from that obtained (Rose, 1981) from the appropriate two-dimensional formulation by Keer *et al.* (1976).

The aim of this paper is to present a fracture analysis of repaired cracks under in-plane mixed-mode loading, focusing first on the special case of isotropic adherends having the same Poisson's ratio, extending the formulation of Keer *et al.* (1976) to include mode II. The problem is reduced to a single integral equation over a finite interval, which permits a parametric study to be performed for the various factors that may influence the repair efficiency. A closed-form solution is also derived for the asymptotic value of the stress intensity factor for long cracks. This asymptotic bound is then extended to include anisotropic reinforcements. Finally comparison with the crack bridging model is made, and it is shown that in the short crack limit the crack bridging model may over-predict the repair efficiency, and hence tends to be non-conservative.

2. FUNDAMENTAL EQUATIONS

Figure 1 shows the repair configuration being considered. Following Keer *et al.* (1976), we will assume that both the cracked plate and the reinforcement are homogeneous, isotropic media. In addition, the adhesive shear stresses are treated as body forces acting on the mid-planes of the bonded plate and reinforcement. It should be noted for one-sided repairs, out-of-plane bending would occur due to the load-path eccentricity (Ratwani, 1978; Wang *et al.*, 1997) so that the coupling between the adherends would involve distributed moments in addition to the in-plane body forces. In the present study, this out-of-plane deformation is ignored for simplicity, as in the previous work of Keer *et al.* (1976), so that the analysis applied strictly to the case of symmetrical reinforcement, i.e. two identical patches are bonded to two sides of the plate, or only one side provided the plate is fully supported against out-of-plane deflection.

For a homogeneous plate, the equations of equilibrium for plane stress conditions are given by the well known Navier's equations in the static case,

$$\nabla^2 \boldsymbol{u} + \frac{1+\nu}{1-\nu}\nabla(\nabla \cdot \boldsymbol{u}) - \boldsymbol{f} = 0 \tag{1}$$

where $\boldsymbol{u}$ represents the displacement vector, $\boldsymbol{f}$ is the body force, and ν is the Poisson's ratio. In the absence of body force, the above equation can be conveniently solved using integral transform methods (Sneddon, 1951; Sneddon and Lowengrub, 1969), with the aid of Airy stress function. In the case of a cracked plate reinforced by a patch, the shear stresses in the adhesive layer can be considered as body forces acting on the mid-planes of the cracked plate and the reinforcement (Keer *et al.*, 1976). Therefore the equations of equilibrium for the crack plate and the reinforcement as depicted in Fig. 1 may be expressed in terms of displacement vectors,

$$\nabla^2 \boldsymbol{u}^{(\mathrm{P})} + \frac{1+\nu_{\mathrm{P}}}{1-\nu_{\mathrm{P}}}\nabla(\nabla \cdot \boldsymbol{u}^{(\mathrm{P})}) - \frac{\gamma_{\mathrm{P}}}{\mu_{\mathrm{P}}}(\boldsymbol{u}^{(\mathrm{P})} - \boldsymbol{u}^{(\mathrm{R})}) = 0, \tag{2}$$

$$\nabla^2 \boldsymbol{u}^{(\mathrm{R})} + \frac{1+\nu_{\mathrm{R}}}{1-\nu_{\mathrm{R}}}\nabla(\nabla \cdot \boldsymbol{u}^{(\mathrm{R})}) - \frac{\gamma_{\mathrm{R}}}{\mu_{\mathrm{R}}}(\boldsymbol{u}^{(\mathrm{R})} - \boldsymbol{u}^{(\mathrm{P})}) = 0. \tag{3}$$

Here and in the following subscripts (or superscripts) P, R, and A are used to distinguish properties pertaining respectively to the plate, the reinforcement, and the adhesive layer. Parameters $\gamma_{P,R}$ describe the shear effect of the adhesive,

$$\gamma_P = \frac{\mu_A}{t_A t_P} \quad \text{and} \quad \gamma_R = \frac{\mu_A}{t_A t_R}, \tag{4}$$

where μ_A is the shear modulus of the adhesive and t_A, t_P, t_R are the thicknesses of the adhesive, the cracked plate and the reinforcement. In general, eqns (2) and (3) are coupled and the solution would normally lead to 2-D integral equations (e.g., Erdogan and Arin, 1972) over the whole extent of the bonded region. In the special case where the cracked plate and the bonded patch have identical Poisson's ratio, Keer *et al.* (1976) showed that, upon subtracting eqn (3) from (2), homogeneous equations can be obtained for the displacement difference vector $\boldsymbol{u}^{(\Delta)}$

$$\frac{2}{1-\nu}\frac{\partial^2 u_x^{(\Delta)}}{\partial x^2} + \frac{\partial^2 u_x^{(\Delta)}}{\partial y^2} + \frac{1-\nu}{1+\nu}\frac{\partial^2 u_y^{(\Delta)}}{\partial x\,\partial y} - \lambda^2 u_x^{(\Delta)} = 0, \tag{5a}$$

$$\frac{\partial^2 u_y^{(\Delta)}}{\partial x^2} + \frac{2}{1-\nu}\frac{\partial^2 u_y^{(\Delta)}}{\partial y^2} + \frac{1-\nu}{1+\nu}\frac{\partial^2 u_x^{(\Delta)}}{\partial x\,\partial y} - \lambda^2 u_y^{(\Delta)} = 0, \tag{5b}$$

where

$$\boldsymbol{u}^{(\Delta)} = \boldsymbol{u}^{(P)} - \boldsymbol{u}^{(R)}, \tag{6}$$

$$\lambda^2 = \frac{\gamma_P}{\mu_P} + \frac{\gamma_R}{\mu_R} \equiv \frac{\mu_A}{t_A}\left(\frac{1}{\mu_P t_P} + \frac{1}{\mu_R t_R}\right). \tag{7}$$

Since eqns (5) are linear partial differential equations with constant coefficients, the unknown displacement difference $\boldsymbol{u}^{(\Delta)}$ can be solved using the Fourier transform technique.

The boundary conditions for the problem shown in Fig. 1(a) are that the surfaces of the crack are stress free and there is a prescribed stress system at infinity so that

$$\sigma_{yy} = \tau_{xy} = 0 \quad (|x| < a, y = 0) \tag{8a}$$

and

$$\sigma_{xx} \to \sigma_{xx}^{\infty}, \quad \sigma_{yy} \to \sigma_{yy}^{\infty}, \quad \tau_{xy} \to \tau_{xy}^{\infty} \quad \text{as} \quad \sqrt{x^2+y^2} \to \infty. \tag{8b}$$

By using the superposition principle it is easy to demonstrate that it is equivalent to solving the following mixed boundary value problem,

$$\sigma_{yy} = -\sigma_0, \quad \tau_{xy} = -\tau_0 \quad (|x| < a, y = 0) \tag{9a}$$

and

$$\sigma_{xx} \to 0, \quad \sigma_{yy} \to 0, \quad \tau_{xy} \to 0 \quad \text{as} \quad \sqrt{x^2+y^2} \to \infty. \tag{9b}$$

In the special case of a single cracked plate, it is obvious that $\sigma_0 = \sigma_{yy}^{\infty}$, $\tau_0 = \tau_{xy}^{\infty}$. For a plate reinforced with a patch, however, the above relationships no longer hold, due to the presence of the reinforcement. Instead the stresses at the prospective location of the crack in a repaired structure would be lower than the remote applied stresses. In general an exact solution for σ_0 and τ_0 is difficult to obtain except for certain simple reinforcement shapes and loads (Rose, 1981). Approximate solutions, however, can be readily derived assuming the stresses in the reinforcement and the base plate are uniform everywhere within the

reinforced portion, and there is no relative displacement between the plate and the reinforcement. Details are presented in Appendix A for the case of an isotropic plate and reinforcement. In the special case that the plate and the reinforcement have identical Poisson's ratio, the prospective tensile and shear stresses are

$$\sigma_0 = \frac{1}{1+S}\sigma_{yy}^{\infty}, \tag{10}$$

$$\tau_0 = \frac{1}{1+S}\tau_{xy}^{\infty}, \tag{11}$$

where $S = E_R t_R / E_P t_P$ denotes the stiffness ratio between the reinforcement and the base plate. The factor $1/(1+S)$ represents the reduction in the plate stress due to the reinforcement.

The boundary value problem represented by eqn (9) can be further decomposed into a tensile mode and a shear mode, according to the superposition principle, i.e.,

$$\sigma_{yy} = -\sigma_0, \quad \tau_{xy} = 0 \quad (|x| < a, y = 0) \quad \text{mode I} \tag{12}$$

and

$$\sigma_{yy} = 0, \quad \tau_{xy} = -\tau_0 \quad (|x| < a, y = 0) \quad \text{mode II}. \tag{13}$$

In the present paper we will assume that the far field stresses are even functions of x, i.e., $\sigma_0(x) = \sigma_0(-x)$ and $\tau_0(x) = \tau_0(-x)$. For mode I loading the displacement u_y is symmetric in x while displacement u_x is anti-symmetric, hence they can be expressed respectively in terms of the Fourier cosine and sine transforms. Details of the solution can be found in Keer *et al.* (1976). The roles of sine and cosine representation should be reversed for mode II as the displacement u_y is anti-symmetric while displacement u_x is symmetric.

3. SOLUTIONS FOR SHEAR MODE

Assuming the reinforced region is infinitely large, the shear mode problem in Fig. 1(a) can be readily reduced to the solution of the perturbation problem shown in Fig. 1(b). where the crack faces are subjected to shear tractions given by eqn (13). Keeping in mind that the shear stress on $y = 0$ is an even function of x, the components of $\boldsymbol{u}^{(\Delta)}$, which satisfy eqn (5), can be represented as follows,

$$u_x^{(\Delta)} = \int_0^{\infty} (A(\xi)\,\mathrm{e}^{-\lambda_1 y} + B(\xi)\,\mathrm{e}^{-\lambda_2 y})\cos(\xi x)\,\mathrm{d}\xi, \tag{14}$$

$$u_y^{(\Delta)} = \int_0^{\infty} C(\xi, y)\sin(\xi x)\,\mathrm{d}\xi, \tag{15}$$

where $A(\xi)$, $B(\xi)$, and $C(\xi, y)$ are functions yet to be determined. Inserting the above expressions into eqn (5), the following equations can be deduced

$$C(\xi, y) = -\frac{\xi}{\lambda_1} A(\xi)\,\mathrm{e}^{-\lambda_1 y} - \frac{\lambda_2}{\xi} B(\xi)\,\mathrm{e}^{-\lambda_2 y}, \tag{16}$$

$$\lambda_1^2 = \xi^2 + \lambda^2, \tag{17}$$

$$\lambda_2^2 = \xi^2 + \frac{1-\nu}{2}\lambda^2. \tag{18}$$

The actual displacements for the cracked plate repaired by a reinforcement can now be expressed as

$$u_x^{(P)} = \alpha u_x^{(\Delta)} + u_x, \tag{19}$$

$$u_y^{(P)} = \alpha u_y^{(\Delta)} + u_y, \tag{20}$$

where u_x and u_y are yet to be determined. Inserting these two equations into (2), it is easy to show that by choosing

$$\alpha = \frac{\gamma_P}{\mu_P \lambda^2}, \tag{21}$$

one obtains the following homogeneous equation,

$$\nabla^2 \boldsymbol{u} + \frac{1+\nu}{1-\nu} \nabla(\nabla \cdot \boldsymbol{u}) = 0, \tag{22}$$

which is exactly the equilibrium equation corresponding to zero body force, for which the general solutions under shear loading are (Sneddon and Lowengrub, 1969)

$$u_x = \frac{1}{2\mu_P} \int_0^\infty \left(\frac{2}{1+\nu} - \xi y \right) \psi(\xi) \, e^{-\xi y} \cos(\xi x) \, d\xi, \tag{23}$$

$$u_y = \frac{1}{2\mu_P} \int_0^\infty \left(\frac{1-\nu}{1+\nu} + \xi y \right) \psi(\xi) \, e^{-\xi y} \sin(\xi x) \, d\xi, \tag{24}$$

where $\psi(\xi)$ is a function yet to be determined. Now the displacements and stresses in the cracked plate can be expressed as

$$u_x^{(P)} = \frac{\gamma_P}{\mu_P \lambda^2} \int_0^\infty (A(\xi) e^{-\lambda_1 y} + B(\xi) e^{-\lambda_2 y}) \cos(\xi x) \, d\xi + \frac{1}{2\mu_P} \int_0^\infty \left(\frac{2}{1+\nu} - \xi y \right) e^{-\xi y} \psi(\xi) \cos(\xi x) \, d\xi, \tag{25}$$

$$u_y^{(P)} = \frac{\gamma_P}{\mu_P \lambda^2} \int_0^\infty \left[-\frac{\xi}{\lambda_1} A(\xi) e^{-\lambda_1 y} - \frac{\lambda_2}{\xi} B(\xi) e^{-\lambda_2 y} \right] \sin(\xi x) \, d\xi + \frac{1}{2\mu_P} \int_0^\infty \left[\frac{1-\nu}{1+\nu} + \xi y \right] e^{-\xi y} \psi(\xi) \sin(\xi x) \, d\xi, \tag{26}$$

$$\sigma_{yy}^{(P)} = \frac{\gamma_P}{\mu_P \lambda^2} \int_0^\infty \frac{2\mu_P}{1-\nu} \left[(-\xi\nu + \xi) A(\xi) e^{-\lambda_1 y} + \left(-\xi\nu + \frac{\lambda_2^2}{\xi} \right) B(\xi) e^{-\lambda_2 y} \right] \sin(\xi x) \, d\xi - \int_0^\infty y \xi^2 \psi(\xi) \, e^{-\xi y} \sin(\xi x) \, d\xi, \tag{27}$$

$$\tau_{xy}^{(P)} = \frac{\gamma_P}{\mu_P \lambda^2} \int_0^\infty \mu_P \left[\left(-\lambda_1 - \frac{\xi^2}{\lambda_1} \right) A(\xi) e^{-\lambda_1 y} - 2\lambda_2 B(\xi) e^{-\lambda_2 y} \right] \cos(\xi x) \, d\xi$$

$$- \int_0^\infty \xi(1-\xi y)\psi(\xi) e^{-\xi y} \cos(\xi x) \, d\xi. \quad (28)$$

Similarly the displacements and stresses in the bonded patch can also be derived, and in particular,

$$u_x^{(R)} = \left(\frac{\gamma_P}{\mu_P \lambda^2} - 1 \right) \int_0^\infty (A(\xi) e^{-\lambda_1 y} + B(\xi) e^{-\lambda_2 y}) \cos(\xi x) \, d\xi$$

$$+ \frac{1}{2\mu_P} \int_0^\infty \left(\frac{2}{1+\nu} - \xi y \right) e^{-\xi y} \psi(\xi) \cos(\xi x) \, d\xi. \quad (29)$$

The mixed boundary conditions for the perturbation problem depicted in Fig. 1(b) are

(i) bonded patch

$$u_x^{(R)} = 0 \quad (-\infty < x < \infty, y = 0), \quad (30a)$$

(ii) cracked plate

$$\sigma_{yy}^{(P)} = 0 \quad (0 \leqslant |x| < a, y = 0), \quad (30b)$$

$$\tau_{xy}^{(P)} = -\tau_0(x) \quad (0 \leqslant |x| < a, y = 0), \quad (30c)$$

$$u_x^{(P)} = 0 \quad (|x| \geqslant a, y = 0). \quad (30d)$$

From these boundary conditions we can determine the remaining three unknown functions $A(\xi)$, $B(\xi)$, and $\psi(\xi)$. In particular, eqn (30b) leads to

$$B(\xi) = -\frac{2\xi^2}{2\xi^2 + \lambda^2} A(\xi), \quad (31)$$

while eqn (30a) results, on making use of eqn (31),

$$\psi(\xi) = -\mu_P(1+\nu) \left(\frac{\gamma_P}{\mu_P \lambda^2} - 1 \right) \frac{A(\xi)\lambda^2}{2\xi^2 + \lambda^2}. \quad (32)$$

The x-displacement and the shear stress in the cracked plate along $y = 0$ are given by

$$u_x^{(P)} = \int_0^\infty U(\xi) \cos(\xi x) \, d\xi, \quad (33)$$

$$\tau_{xy}^{(P)} = -\frac{\gamma_P}{\lambda^2}(1+\nu) \int_0^\infty [F_{II}(\xi) - \xi] U(\xi) \cos(\xi x) \, d\xi - \int_0^\infty \mu_P(1+\nu)\xi U(\xi) \cos(\xi x) \, d\xi, \quad (34)$$

where

$$U(\xi) = \frac{\lambda^2}{2\xi^2 + \lambda^2} A(\xi), \tag{35}$$

$$F_{II}(\xi) = \frac{(2\xi^2 + \lambda^2)^2 - 4\lambda_1\lambda_2\xi^2}{(1+\nu)\lambda_1\xi}. \tag{36}$$

Here the subscript "II" is used to signify quantities pertaining to mode II. It is easy to see that F_{II} differs from its counterpart for mode I (Keer *et al.*, 1976), which is given in Appendix B expressed in accordance with the present notation. The implications of this difference will be discussed later.

Boundary condition (30d) can be automatically satisfied if we represent function $U(\xi)$ by the following integral (Sneddon and Lowengrub, 1969)

$$U(\xi) = \int_0^a \Phi(t) J_0(\xi t)\, dt, \tag{37}$$

where $J_0(x)$ is the Bessel function of zero order. So the shear stress in the cracked plate along $y = 0$ is

$$\begin{aligned}\tau_{xy}^{(P)} &= -\frac{\gamma_P}{\lambda^2}(1+\nu)\int_0^\infty (F_{II}(\xi) - \xi) U(\xi)\cos(\xi x)\, d\xi - \frac{d}{dx}\int_0^\infty \mu_P(1+\nu) U(\xi)\sin(\xi x)\, d\xi \\ &= -\frac{\gamma_P}{\lambda^2}(1+\nu)\int_0^\infty (F_{II}(\xi) - \xi) U(\xi)\cos(\xi x)\, d\xi - \frac{d}{dx}\int_0^a \mu_P(1+\nu)\Phi(t)\frac{H(x-t)}{\sqrt{x^2-t^2}}\, dt,\end{aligned} \tag{38}$$

where the identity (Erdelyi, 1954)

$$\int_0^\infty J_0(\xi t)\sin(\xi x)\, d\xi = \frac{H(x-t)}{\sqrt{x^2-t^2}} \tag{39}$$

has been used. Here H is the Heaviside function. Therefore the boundary condition (30c) can be expressed as

$$-\tau_0(x) = -\frac{d}{dx}\int_0^x \frac{\mu_P(1+\nu)\Phi(t)}{\sqrt{x^2-t^2}}\, dt - \frac{\gamma_P}{\lambda^2}(1+\nu)\int_0^\infty (F_{II}(\xi) - \xi) U(\xi)\cos(\xi x)\, d\xi, \tag{40}$$

which is an Abel integral equation, which can be solved to yield the following Fredholm integral equation of the second kind:

$$\mu_P(1+\nu)\Phi(r) + \frac{\gamma_P}{\lambda^2} r(1+\nu)\int_0^a L_{II}(t,r)\Phi(t)\, dt = \frac{2}{\pi} r\int_0^r \frac{\tau_0(t)}{\sqrt{r^2-t^2}}\, dt, \tag{41}$$

where

$$L_{II}(t,r) = \int_0^\infty (F_{II}(\xi) - \xi) J_0(\xi t) J_0(\xi r)\, d\xi. \tag{42}$$

In the case of constant shear stress $\tau_0(x) = \tau_0$, we obtain the following integral equation,

$$\Phi(r) + \frac{S}{1+S} r\int_0^a L_{II}(t,r)\Phi(t)\, dt = \frac{\tau_0 r}{(1+\nu)\mu_P}. \tag{43}$$

For comparison, the integral equation for mode I loading is also given in Appendix B, where the present notation has been used. The similarity between mode I and mode II is

apparent, but the above mentioned difference between the two functions F_{II} and F_I has a significant implication for the repair efficiency under mode II relative to mode I, as discussed in Section 4.

The stress intensity factor at the crack tip can be determined either using displacement or stress based definitions, i.e., eqn (33) or (38); both methods yield the same result. Here we will take the former approach,

$$K_{II} = \lim_{x \to a^-} (1+\nu)\mu_P \sqrt{\frac{\pi}{2}} \frac{u_x^{(P)}}{\sqrt{a-x}}. \tag{44}$$

Noting eqns (33) and (37) and after integration by parts to isolate the singularity term, we have

$$K_{II} = (1+\nu)\mu_P \sqrt{\pi} \frac{\Phi(a)}{\sqrt{a}}. \tag{45}$$

It is easy to verify that the unrepaired situation can be recovered as a special case, by setting $\lambda = 0$, so that

$$L_{II}(t, r) = 0 \tag{46}$$

in eqn (43), and thus

$$\Phi(a) = \frac{\tau_0 a}{(1+\nu)\mu_P}, \tag{47}$$

$$K_{II} = \tau_0 \sqrt{\pi a}. \tag{48}$$

It should be emphasised that the stress intensity factor given by eqn (45) represents the second stage analysis of a bonded repair (Rose, 1981, 1985); the contribution of stage one to the reduction in stress intensity factor is reflected by the lower tractions applied to the crack faces as compared prior to patching, see eqn (11).

4. NUMERICAL RESULTS

The integral eqn (43) can be readily solved as it is non-singular, and the kernel, eqn (42), converges rapidly for arbitrary t and r. In the present work the integral equation was solved using the Gauss–Legendre method, and the value of Φ at $x = a$ was evaluated using the Nystrom's interpolation method (Press *et al.*, 1992). A convergence study showed that an accuracy of 0.1% in the stress intensity factor can be achieved for $N = 50$, with crack lengths up to $ka \leqslant 20$ (k is a characteristic spring constant to be discussed later). The order of the Gauss–Legendre integration method needs to be increased should the stress intensity factors for even longer crack lengths be required. As will be seen later, this is generally unnecessary as the stress intensity factor for a crack length corresponding to the above chosen limit approaches 99.95% of the limiting value for semi-infinite crack length.

As an example, the problem was solved for the following materials and dimensions, typifying a bonded patch used in repairing aircraft structures (see e.g. Baker and Jones, 1988):

Cracked plate: $E_P = 72$ GPa, $t_P = 3.0$ mm

Patch: $E_R = 208$ GPa, $t_R = 1.0$ mm

Adhesive: $\mu_A = 0.7$ GPa, $t_A = 0.2$ mm

and the Poisson's ratio is taken to be 0.3 for both the cracked plate and the patch. Here we assume that the patch can be considered as an isotropic material; the effect of anisotropy

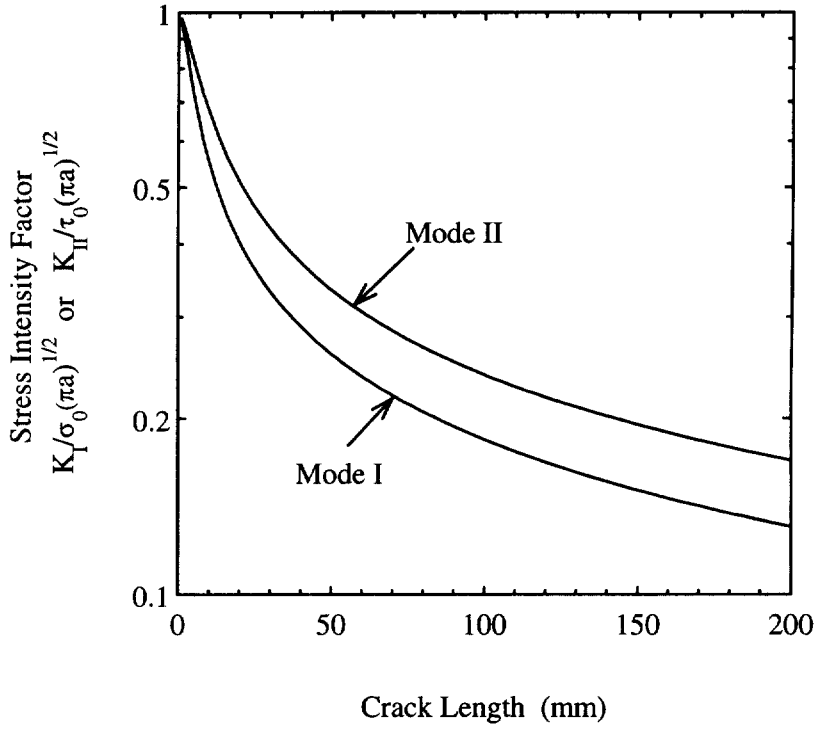

Fig. 2. Reduction in mode I and mode II stress intensity factors due to bonded repair, for typical values of plate and patch parameters.

will be discussed later. The stress intensity factors K_{II} obtained from eqn (43) for various crack lengths are plotted in Fig. 2. The numerical results are given as the ratio of the stress intensity factor after and before repair. It is clear that there is a significant reduction in the stress intensity factor after reinforcement, the reduction increasing with increasing crack length. For comparison, the stress intensity factor for mode I loading is also shown in the figure, indicating a higher reduction ratio under mode I than mode II.

The numerical results revealed a very interesting and unexpected difference between the asymptotic behaviours of mode I and mode II stress intensity factors. In the case of a single sheet containing a crack, the intensity factors under tensile and shear modes have the same functional form, i.e.

$$\frac{K_I}{\sigma} = \frac{K_{II}}{\tau} = \sqrt{\pi a}. \tag{49}$$

However, for a repaired crack, the normalised stress intensity factor exhibits a different behaviour as the crack length increases, as shown in Fig. 3,

$$\frac{K_I(a)}{\sigma_0} \leqslant \frac{K_{II}(a)}{\tau_0}. \tag{50}$$

The dashed lines in the figure represent asymptotic values for mode I and mode II, respectively; the derivations are given in the next section. In the long crack limit, the asymptotic value for mode II is significantly higher than mode I; the difference (which depends on the Poisson's ratio, as will be shown later) in the present example is approximately 35%. This difference would certainly impact on the design of bonded patches for mixed mode loading situations, and is indicative of a different reinforcement mechanism for shear loading as compared with the tensile mode. Further discussion concerning the limiting case when the crack length approaches infinity will be presented in the next section, as it permits an

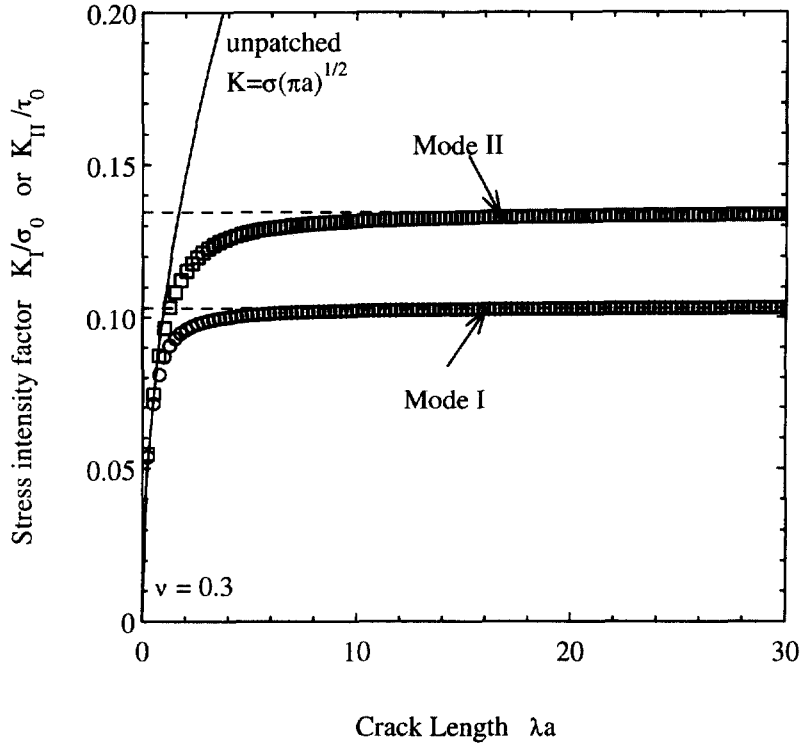

Fig. 3. Asymptotic behaviour of mode II and mode I stress intensity factors versus crack length. Symbols: solution of integral eqns (43) and (B3). Dashed lines: asymptotic values.

independent, one-dimensional analysis to be carried out for the energy release rate, and hence for the stress intensity factors.

5. ASYMPTOTIC SOLUTION FOR LONG CRACK LIMIT

Although the integral eqn (43) can be solved using an asymptotic expansion method for the small crack limit (i.e., $a \to 0$) (Rose, 1982), there appears to be no effective method for handling the long crack limit ($a \to \infty$). An alternative method is to determine the energy release rate for a semi-finite crack subjected to in-plane shear using an energy approach. A two-dimensional idealisation of a representative bonded joint subjected to shear loading is schematically shown in Fig. 4. By definition, the energy release rate is given by $G = -\partial\Pi/2t_P\partial a$, where Π is the potential energy of the system. In the case of linear elastic systems, the strain energy release rate, $G_{II,\infty}$, for a semi-infinite crack can be determined by considering the energy required to re-close a strip, thus,

$$G_{II,\infty} t_P = \tau_0 u_x(y = 0) t_P, \tag{51}$$

where the sliding displacement $u_x(y = 0)$ is the x-displacement of the loaded adherend shown in Fig. 4. In the following we will first consider the case of plate and reinforcement being isotropic in keeping with the preceding analysis; an extended solution is presented in the next section to incorporate the effect of anisotropy in either the plate or the reinforcement.

For a semi-infinite crack along $x < 0$, $y = 0$, all the strain components pertaining to the plate and the reinforcement should be position independent in the x-direction for both limits $x \to \infty$ and $x \to -\infty$, i.e.,

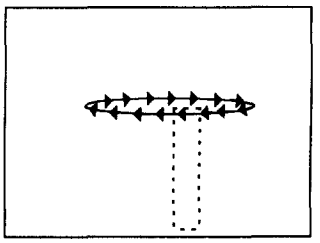

(a)

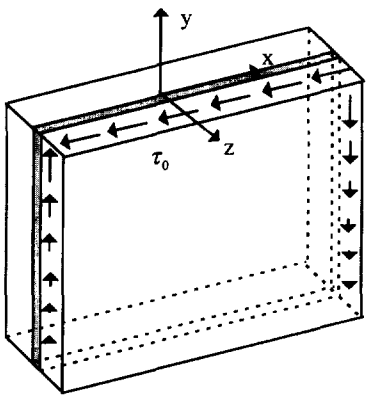

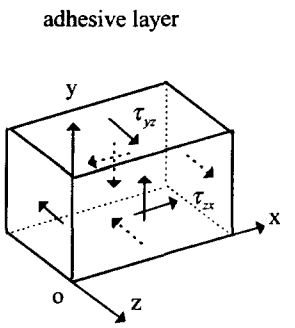

(b) (c)

Fig. 4. (a) A repaired crack subjected to shear loading, (b) representative bonded joint under in-plane shear, and (c) stresses in the adhesive layer.

$$\frac{\partial^2 u_x^{(P)}}{\partial x^2} = \frac{\partial^2 u_y^{(P)}}{\partial x\,\partial y} = \frac{\partial^2 u_x^{(R)}}{\partial x^2} = \frac{\partial^2 u_y^{(R)}}{\partial x\,\partial y} = 0, \tag{52}$$

hence eqns (2) and (5a) reduce to

$$\frac{\partial^2 u_x^{(P)}}{\partial y^2} - \frac{\gamma_P}{\mu_P} u_x^{(\Delta)} = 0, \tag{53}$$

$$\frac{\partial^2 u_x^{(\Delta)}}{\partial y^2} - \lambda^2 u_x^{(\Delta)} = 0, \tag{54}$$

which lead to the following solutions that remain bounded in the domain $y \leqslant 0$,

$$u_x^{(\Delta)} = A\,e^{\lambda y}, \tag{55}$$

$$u_x^{(P)} = \frac{\gamma_P}{\mu_P}\frac{A}{\lambda^2} e^{\lambda y} + By + C, \tag{56}$$

where constants A, B and C are unknown constants yet to be determined. Since the displacement $u_x^{(P)}$ should vanish as $y \to -\infty$, constants B and C should be zero. Other boundary conditions for the reinforcement and the plate are

$$u_x^{(R)} = 0 \quad \text{at} \quad y = 0, \tag{57}$$

$$\tau_{xy}^{(P)} = \tau_0 \quad \text{at} \quad y = 0. \tag{58}$$

So the following solutions can be obtained, noting that $\tau_{xy}^{(P)} = \mu_P \partial u_x^{(P)}/\partial y$

$$u_x^{(P)} = \frac{\lambda}{\gamma_P}\tau_0 e^{\lambda y}. \tag{59}$$

Consequently the crack sliding displacement is

$$u_x^{(P)}(y = 0) = \frac{\lambda}{\gamma_P}\tau_0 = \frac{\lambda}{\mu_A} t_A t_P \tau_0. \tag{60}$$

With this, the strain energy release rate can be derived

$$G_{II,\infty} = \frac{1}{t_P}\tau_0 t_P u_x^{(P)}(y = 0) \equiv (\tau_0)^2 \lambda t_P \frac{t_A}{\mu_A}. \tag{61}$$

Using Irwin's relation, the mode II stress intensity factor is thus

$$K_{II,\infty} = \sqrt{E_P G_{II,\infty}} \equiv \tau_0 \sqrt{E_P \frac{t_A}{\mu_A}\lambda t_P} = \frac{\tau_0[2(1+\nu)(1+S)]^{1/2}}{\sqrt{\lambda S}}, \tag{62}$$

where

$$S = \frac{\mu_R t_R}{\mu_P t_P} = \frac{E_R t_R}{E_P t_P}. \tag{63}$$

For the purpose of comparison with mode I (Rose, 1982), eqn (62) can be rewritten as

$$K_{II,\infty} = \tau_0/\sqrt{k_{II}}, \tag{64}$$

where k_{II} represents a spring constant for shear mode,

$$k_{II} = \frac{\lambda S}{2(1+\nu)(1+S)}. \tag{65}$$

It is evident that the shear spring constant given by eqn (65) is dependent on the shear moduli and Poisson's ratio of the cracked plate and the reinforcement. As will be discussed later, for an isotropic material this shear spring constant is smaller than the spring constant corresponding to mode I, as the shear stiffness is apparently lower than tensile stiffness. Consequently the limiting value of mode II stress intensity factor of a repaired crack is greater than under tensile mode. One important implication arising from this difference is that when strongly anisotropic reinforcements with low in-plane shear moduli, such as unidirectional plastic reinforced composites, are used to repair a crack under shear loading, the repair efficiency will be much lower than could be expected on the basis of mode I analysis.

6. ORTHOTROPIC REINFORCEMENT

Frequently fibre reinforced composite patches (Baker and Jones, 1988) are used in bonded repairs due to their highly desirable structural properties. In particular, boron–epoxy is currently the most widely used reinforcement in repairing aircraft structures due

to the non-conductivity of the boron–epoxy composite, thus permitting the use of the eddy-current method to measure crack length. When the crack to be repaired is under mode I loading, the use of unidirectional boron–epoxy composites with the fibre direction being perpendicular to the crack is shown to provide the maximum reinforcement in reducing the stress intensity factor. However, in the case of shear loading, the same method may become less effective due to the low in-plane shear modulus of the composite material. Detailed analysis will be presented below.

For the representative joint shown in Fig. 4, since the displacements in the plate and the reinforcement are position independent in the x direction, the two in-plane shear strains in the plate and the patch may be expressed as,

$$\gamma_{xy}^{(P)} \equiv \frac{du_x^{(P)}}{dy} = \frac{\tau_{xy}^{(P)}}{\mu_{P,xy}}, \tag{66}$$

$$\gamma_{xy}^{(R)} \equiv \frac{du_x^{(R)}}{dy} = \frac{\tau_{xy}^{(R)}}{\mu_{R,xy}}, \tag{67}$$

where the in-plane shear moduli of the plate and the reinforcement are designated as $\mu_{P,xy}$ and $\mu_{R,xy}$, respectively. The equations of equilibrium of the plate and the reinforcement in the x direction lead to, treating the adhesive stresses as body forces acting on the mid-planes of the reinforcement and the plate,

$$\frac{\partial \tau_{xy}^{(P)}}{\partial y} = f_{x,P} \equiv \frac{\tau_{xz}^{(A)}}{t_P}, \tag{68}$$

$$\frac{\partial \tau_{xy}^{(R)}}{\partial y} = f_{x,R} \equiv -\frac{\tau_{xz}^{(A)}}{t_R}, \tag{69}$$

where $f_{x,P}$ and $f_{x,R}$ represent the body forces for the plate and the reinforcement, which in the present case are equal to the shear stresses in the adhesive layer, divided by the plate and reinforcement thicknesses. Since the shear strain in the adhesive layer is

$$\gamma_{xz}^{(A)} = \frac{u_x^{(P)} - u_x^{(R)}}{t_A}, \tag{70}$$

differentiating eqn (70) we have, noting eqns (66) and (67)

$$\frac{d^2\tau_{xz}^{(A)}}{dy^2} = \frac{\mu_A}{t_A}\left(\frac{d^2u_x^{(P)}}{dy^2} - \frac{d^2u_x^{(R)}}{dy^2}\right) \equiv \frac{\mu_A}{t_A}\left(\frac{d\gamma_{xy}^{(P)}}{dy} - \frac{d\gamma_{xy}^{(R)}}{dy}\right). \tag{71}$$

Using eqns (68) and (69) the governing equation for the adhesive shear stress becomes

$$\frac{d^2\tau_{xz}^{(A)}}{dy^2} = \lambda^2 \tau_{xz}^{(A)}, \tag{72}$$

where

$$\lambda^2 = \frac{\mu_A}{t_A}\left[\frac{1}{\mu_{P,xy}t_P} + \frac{1}{\mu_{R,xy}t_R}\right]. \tag{73}$$

The solution for eqn (72) which remains bounded in the half plane $y < 0$ is

$$\tau_{xz}^{(A)} = \tau_{max}\, e^{\lambda y}, \tag{74}$$

where τ_{max} can be determined from the following boundary condition, making use of eqns (66–70)

$$\left.\frac{d\tau_{xz}^{(A)}}{dy}\right|_{y=0} = \mu_A \left.\frac{d\gamma_{xz}^{(A)}}{dy}\right|_{y=0} = \frac{\mu_A}{t_A}\left.\left(\frac{du_x^{(P)}}{dy} - \frac{du_x^{(R)}}{dy}\right)\right|_{y=0} = \tau_0 t_P \lambda^2. \tag{75}$$

Therefore from eqn (74)

$$\tau_{max} = \lambda t_P \tau_0. \tag{76}$$

The sliding displacement is thus, noting eqn (70)

$$u_x^{(P)}(y=0) = \gamma_{max} t_A = \frac{\tau_0}{\mu_A} \lambda t_A t_P, \tag{77}$$

which is the same as eqn (60) for the isotropic case, except that the characteristic parameter λ now takes a more general definition in terms of the in-plane shear moduli of the plate and the reinforcement, see eqn (73). Therefore the result obtained previously for isotropic plate and reinforcement, i.e. eqn (62), is still applicable to anisotropic reinforcements, providing the appropriate in-plane shear moduli for the plate and the reinforcement are used to compute the shear transfer parameter λ.

Now let us consider an example of using unidirectional boron–epoxy composite as reinforcement to repair a mode II crack. The shear modulus of a typical boron–epoxy patch (Baker and Jones, 1988) is around 7.0 GPa, while the Young's modulus in the fibre direction is approximately 208 GPa, with the Poisson's ratio being about 0.18. The dimensions and material properties for the cracked plate were the same as the example considered in Section 4. The asymptotic value of the mode II stress intensity factor determined from eqn (64) (using the shear transfer parameter given by eqn (73)) is shown by the dashed curve in Fig. 5, together with the stress intensity under mode I loading. It is clear that the asymptotic

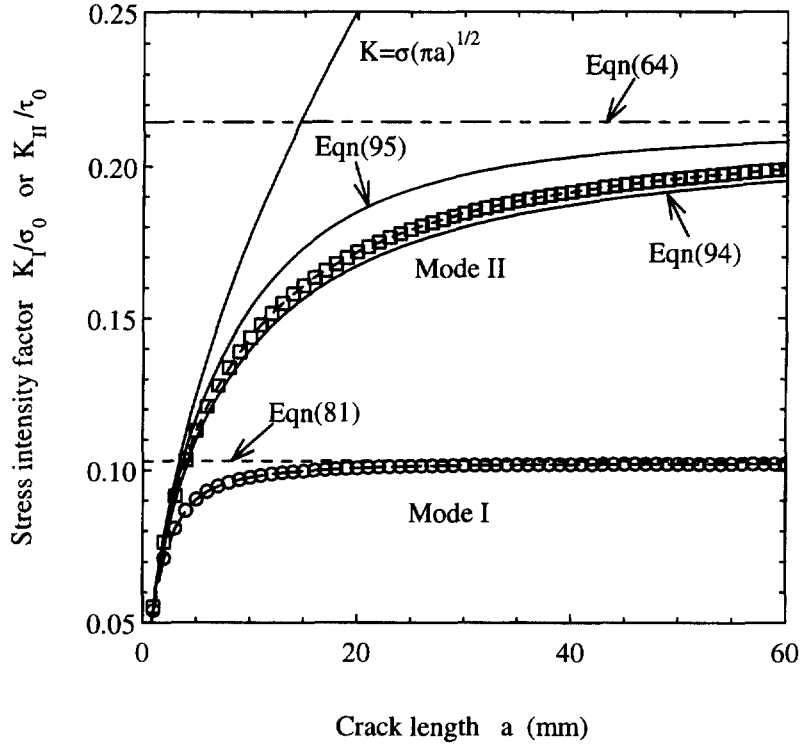

Fig. 5. Repair performance of orthotropic patches under mode II and mode I.

value of the mode II stress intensity factor is much higher than mode I. By approximating the reinforcement as an isotropic material, the mode I and mode II stress intensity factors can be evaluated using the integral equation approach for arbitrary crack length; the results are also shown in Fig. 5 by symbols. The crack length at which the mode II stress intensity factor approaches the asymptotic value is much longer than the characteristic crack length of mode I. In the context of composite patch repair, this means that in the short crack limit reinforcement is far less effective for the shear mode than tensile mode. These results help to explain the finite element results of a patched crack under biaxial loading obtained by Chue *et al.* (1994), who reported that the repair efficiency for mode II was much lower than under mode I.

7. SPRING CONSTANT FOR MODE I

From the foregoing analysis using integral transform formulation, three essential parameters have been identified that would influence the stress intensity factor (both mode I and mode II) of a patched crack. These are, the shear transfer length (β^{-1} for mode I and λ^{-1} for mode II), stiffness ratio (S), and Poisson's ratio (ν). In the crack bridging model (Rose, 1987) the only characteristic parameter is the spring constant, k, although this spring constant is a compound of all the three parameters, see eqn (65) for mode II. However, the mode I spring constant used earlier by Rose (1982) was based on the standard engineering approximation, which treats the representative bonded joint as being under plane stress conditions. Careful re-examination of this approach appears to suggest that plane strain assumption would be more appropriate for the problem, as the displacements should be position independent along the x direction (McCartney (1992) has suggested a concept of generalised plane strain condition for the analogous problem of matrix cracking in $0°/90°$ laminates). To illustrate this point, let us first consider the field equations governing the deformation of a strip representing the centre region of an infinite crack as depicted in Fig. 4, except that the joint is now subjected to a normal stress along $y = 0$. All the strain components pertaining to the plate and the reinforcement should be position independent in the x-direction, i.e., the strip should be considered as under generalised plane strain. Consequently eqn (5b) reduces to

$$\frac{2}{1-\nu}\frac{\partial^2 u_y^{(\Delta)}}{\partial y^2} - \lambda^2 u_y^{(\Delta)} = 0, \tag{78}$$

which has the following solution in the $y < 0$ domain

$$u_y^{(\Delta)}(y) = A\, e^{\beta^* y}, \tag{79}$$

where A is an unknown constant yet to be determined, and

$$\beta^* = \left[\frac{\mu_A}{t_A}\left(\frac{1-\nu^2}{E_P t_P} + \frac{1-\nu^2}{E_R t_R}\right)\right]^{1/2}, \tag{80}$$

for isotropic adherends. When compared with the load transfer parameter used by Rose (1982, 1988), the present result shows that the Young's moduli of the plate and the reinforcement should be replaced by the plane-strain moduli. When this new expression is used, the stress intensity factor can be expressed as

$$K_{I,\infty} = \sqrt{E_P G_\infty} = \frac{\sigma_0}{\sqrt{k_I}}, \tag{81}$$

where k_I is given by

$$k_{\mathrm{I}} = \frac{\beta^* S}{(1+S)(1-\nu^2)} = \frac{\lambda S}{\sqrt{2}(1+\nu)\sqrt{1-\nu}(1+S)} = \sqrt{\frac{2}{1-\nu}}\, k_{\mathrm{II}}, \tag{82}$$

which is greater than that obtained by Rose (1981, 1988) by a factor $\sqrt{1-\nu^2}$. It is also clear that the mode I spring constant is greater than its mode II counterpart by a factor of $\sqrt{2/(1-\nu)}$, implying that an isotropic patch would have a higher repair efficiency under mode I than under shear mode. In terms of the stress intensity factor, the minimum ratio between mode II and mode I stress intensity factors is $\sqrt[4]{2} \approx 1.19$ for $\nu = 0$, and the maximum ratio is $\sqrt{2} \approx 1.414$ for $\nu = 0.5$.

To demonstrate the validity of the present results, numerical results of the integral equations for mode II (see eqn (43)) and mode I (see Appendix B) are presented as curves in Fig. 6 showing the influence of Poisson's ratio on the asymptotic stress intensity factors in the long crack limit $a \to \infty$. In the numerical study the stress intensity factors were computed at a crack length corresponding to $ka = 20$. The stress intensity factor at this crack length is estimated to approach 99.95% of the asymptotic value. Only the Poisson's ratio was varied while the Young's moduli and geometrical dimensions were kept the same as those given in Section 3. Two different trends can be observed in Fig. 6. First, the mode II stress intensity factor increases as the Poisson's ratio increases, and such an increase is well predicted by the upper bound solutions (eqn (62)). The reason for the observed increase is primarily due to the decrease in the shear modulus as the Poisson's ratio increases while the Young's moduli are kept constant. Secondly, the mode I stress intensity factor actually decreases with an increase in the Poisson's ratio. The reduction in the mode I stress intensity factor is, however, not expected from the earlier asymptotic solution by Rose (1982, 1987). It is therefore evident that the plane stress assumption for the representative bonded joint was inadequate. It is also clear from Fig. 6(b) that the decrease in the mode I stress intensity factor as the Poisson's ratio increases is well predicted by the present spring constant, given by eqn (82).

An alternative method for determining the spring constant without resorting to the solution of representative bonded joints is as follows. For mode I, the spring constant is defined by (Rose, 1987)

$$k = \frac{\sigma_0}{E_{\mathrm{P}} u_y}, \tag{83}$$

which may be expressed as

$$k = \lim_{\xi \to 0} \frac{\hat{\sigma}(\xi)}{E\hat{u}(\xi)}, \tag{84}$$

where

$$\hat{\sigma}(\xi) = \int_0^\infty \sigma_{yy}(x) \cos(\xi x)\, \mathrm{d}x$$

and

$$\hat{u}(\xi) = \int_0^\infty u_y(x) \cos(\xi x)\, \mathrm{d}x$$

are the Fourier cosine transforms of the stress and displacement. This can be interpreted as applying a periodic pressure of infinite wavelength (or zero wave-number) to the edge $y = 0$ of a reinforced half-plate (Rose, 1982). Then the spring constant is defined by the ratio between the stress and displacement. From eqns (26) and (27) in Keer *et al.* (1976) we have

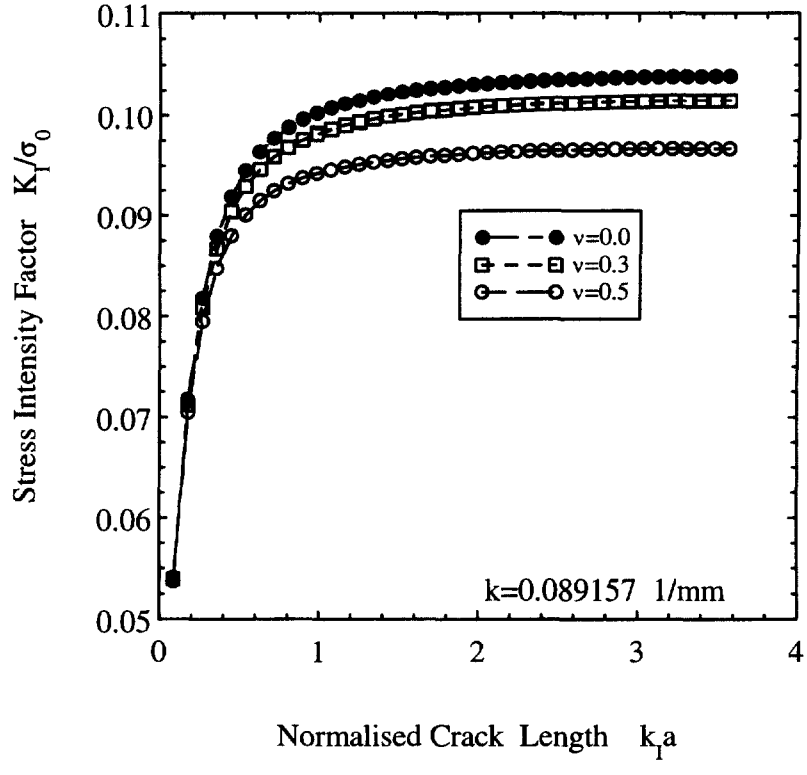

(a)

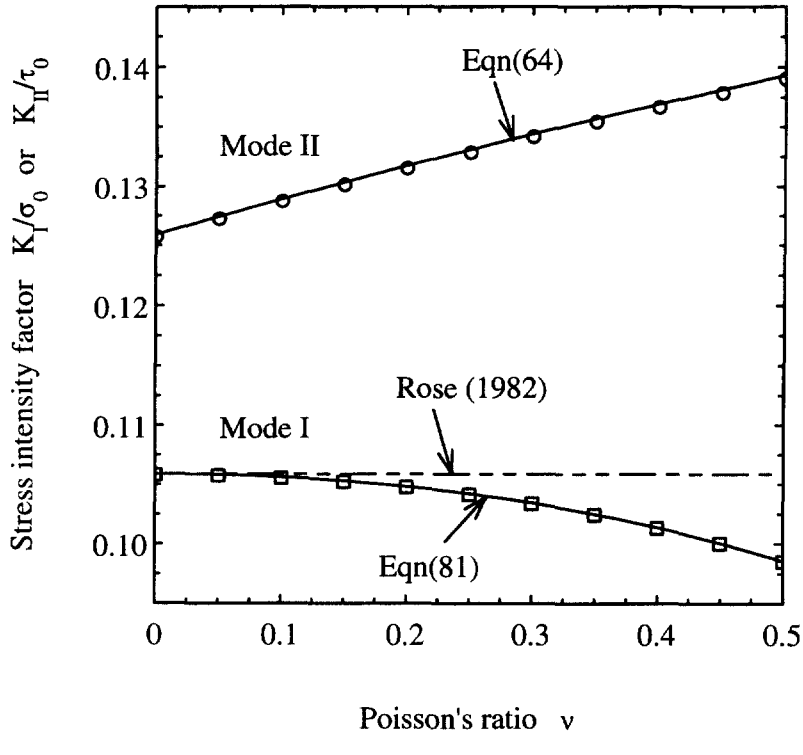

(b)

Fig. 6. Influence of Poisson's ratio on the asymptotic stress intensity factors, (a) asymptotic behaviour and (b) limiting value in the long crack limit. Symbols: exact solution of integral equations; solid curves: closed form solutions.

$$\hat{\sigma}\frac{1}{(1+\nu)\mu_P} = -\xi\hat{u} - \frac{S}{1+S}[F_I(\xi)-\xi]\hat{u} \tag{85}$$

for mode I, and from eqns (33) and (34)

$$\hat{\tau}\frac{1}{(1+\nu)\mu_P} = -\xi\hat{u} + \frac{S}{1+S}[F_{II}(\xi)-\xi]\hat{u} \tag{86}$$

for mode II. Combining eqns (85) and (86) with eqn (84) the following spring constants can be readily derived

$$k_I = \frac{\lambda S}{\sqrt{2}(1+\nu)\sqrt{1-\nu}(1+S)} \tag{87}$$

and

$$k_{II} = \frac{\lambda S}{2(1+\nu)(1+S)}, \tag{88}$$

which are respectively identical to eqns (82) and (65), confirming the validity of the spring constants derived earlier from representative overlap joints under plane strain condition.

8. COMPARISON WITH CRACK BRIDGING MODELS

It is interesting to note that both the mode I and mode II spring constants, k_I and k_{II}, contain all the three variables identified in Section 7, and it is not unreasonable to expect that the behaviour in the long crack limit (Rose, 1987) is characterised by these spring constants. The short crack limit, however, may behave differently from what would be predicted by the crack bridging model, which has only one scaling parameter, the spring constant.

In the short crack limit, $a \to 0$, the integral eqn (43) is amenable to successive solution (Rose, 1982), which leads to

$$K_{I,II}(a) = \sigma_0\sqrt{\pi a}\left[1 + \frac{A_{I,II}}{2}\frac{S}{1+S}a^2\ln a + O(a^2)\right], \tag{89}$$

where

$$A_{I,II} = \lim_{\xi\to\infty}\xi[F_{I,II}(\xi)-\xi] = \frac{1}{8(1+\nu)}[8+(1+\nu)^2]\lambda^2. \tag{90}$$

It is noted that in the short crack limit, the repair efficiency under mode I is identical to that under mode II. It is also clear that the spring constant (k_I or k_{II}) are not the only scaling parameter that characterises the transient behaviour for short crack lengths. In fact, the three parameters cannot be lumped into a single spring constant, as the stiffness ratio S and the Poisson's ratio ν also affect the repair efficiency. This is demonstrated in Fig. 7, where the symbols represent the exact solution of the integral equation, and the dashed line denotes the solution of the crack bridging model using the presently derived spring constant. As expected, the crack bridging model gives the same results as the present method in the limiting condition of $S \to 0$ or $\beta^{-1}/k_I^{-1} \to 0$, i.e. the shear transfer length is far smaller than the characteristic crack length (k_I^{-1}). The ratio between the shear transfer length and the characteristic crack length is, according to eqn (82),

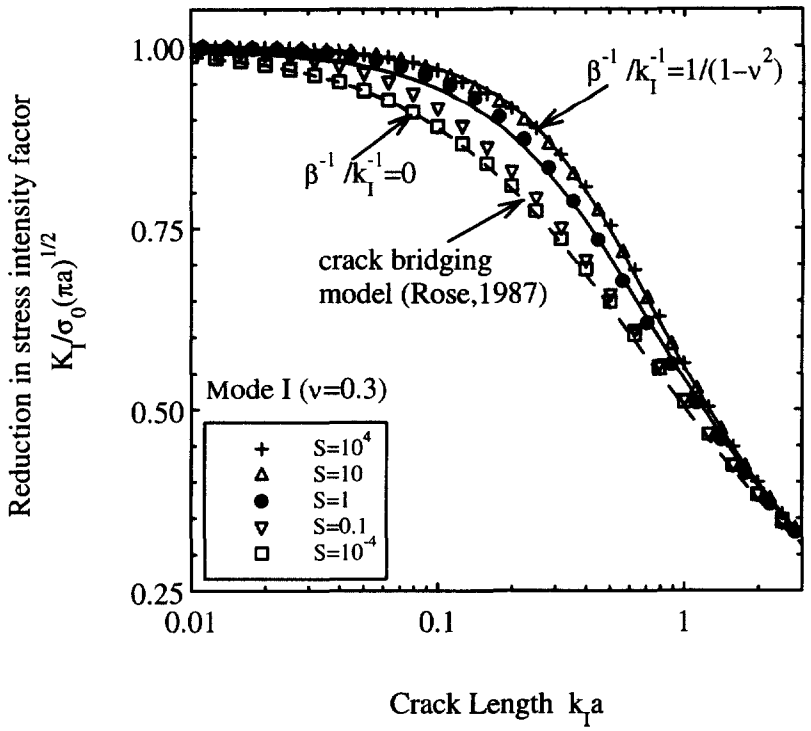

Fig. 7. Comparison between present method and crack bridging model for various patch geometries. Symbols: exact solution of the integral equation; dashed curve: solution of crack bridging model. Solid curves: eqn (95).

$$\frac{\beta^{-1}}{k_I^{-1}} = \frac{S}{(1-\nu^2)(1+S)} \tag{91}$$

for mode I and, noting eqn (65),

$$\frac{\lambda^{-1}}{k_{II}^{-1}} = \frac{S}{2(1+\nu)(1+S)} \tag{92}$$

for mode II. The two extreme cases are (i) a cracked plate reinforced by a patch with a stiffness far less than plate, i.e., $S \to 0$ leading to $\beta^{-1}/k_I^{-1} \to 0$. (ii) The reinforcement is absolutely rigid. $S \to \infty$, leading to $\beta^{-1}/k_I^{-1} \to 1/(1-\nu^2)$. As evidenced in Fig. 7, the repair efficiency is highest for the former case and lowest for the latter, although the two cases converge in the long crack limit. Strictly speaking the crack bridging method (Rose, 1987) is accurate only for the special case of $\beta^{-1}/k_I^{-1} \to 0$ ($S \to 0$), i.e., the elastic stiffness of the cracked plate is far greater than that of the reinforcement. For other cases, the crack bridging model over-predicts the reinforcement efficiency, hence tends to be somewhat non-conservative.

Based on the crack bridging model, Rose (1987) constructed an interpolating equation (corresponds to the limiting case $\beta^{-1}/k_I^{-1} \to 0$), as depicted in Fig. 7,

$$K_I = \sigma_0 \sqrt{\pi a} F_I(k_I a), \tag{93}$$

where

$$F_1(x) = \sqrt{\frac{1+px}{1+(p+8/\pi)x+p\pi x^2}}, \tag{94}$$

where for a fully bridged crack, $p = (2A_2\pi^2 - 48)/(8\pi - \pi^3)$ and $A_2 = 1.768$. This formula is shown in Fig. 7. In practical applications of crack patching, the most common practice is to design a patch so that $S = 1.0$ (Baker and Jones, 1988). For this case, the following interpolating equation appears to provide a better correlation with the numerical results shown in Fig. 7,

$$F_1(x) = \left[\frac{\tanh(\pi x/(1+B\pi x))}{\pi x}\right]^{1/2}, \tag{95}$$

where constant B has been determined by curve fitting the numerical solution of the integral equation, which gives $B = 0.1$ for $S \to \infty$ and $B = 0.3$ for $S = 1.0$.

9. DISCUSSION AND CONCLUSIONS

Now that we have established the influences of the shear transfer length (β^{-1} for mode I and λ^{-1} for mode II) and the characteristic crack length (k^{-1}) on the efficiency of crack patching, the effect of the third parameter, the Poisson's ratio, can be readily evaluated. For simplicity sake we will consider only the case of mode I with a stiffness ratio $S = 1.0$. The reductions in stress intensity factor for three different Poisson's ratios are plotted in Fig. 8. The results obtained from the integral equation cannot be distinguished from these curves on the scale of Fig. 8, thus it is not unreasonable to conclude that the effect of Poisson's ratio is fully captured by the spring constant, which varies with the Poisson's ratio according to eqns (65) and (82). Similarly, when the crack lengths are normalised by the respective spring constants, there is no discernible difference between the mode I and

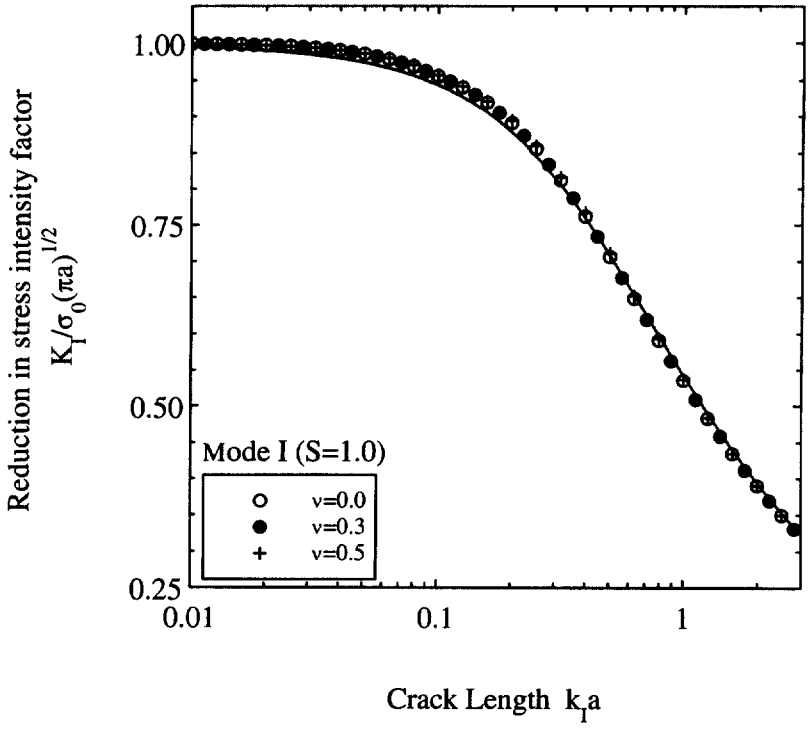

Fig. 8. Influence of Poisson's ratio on the stress intensity factor after patching. Symbols: exact solutions of the integral equation (mode I); solid curve: eqn (95).

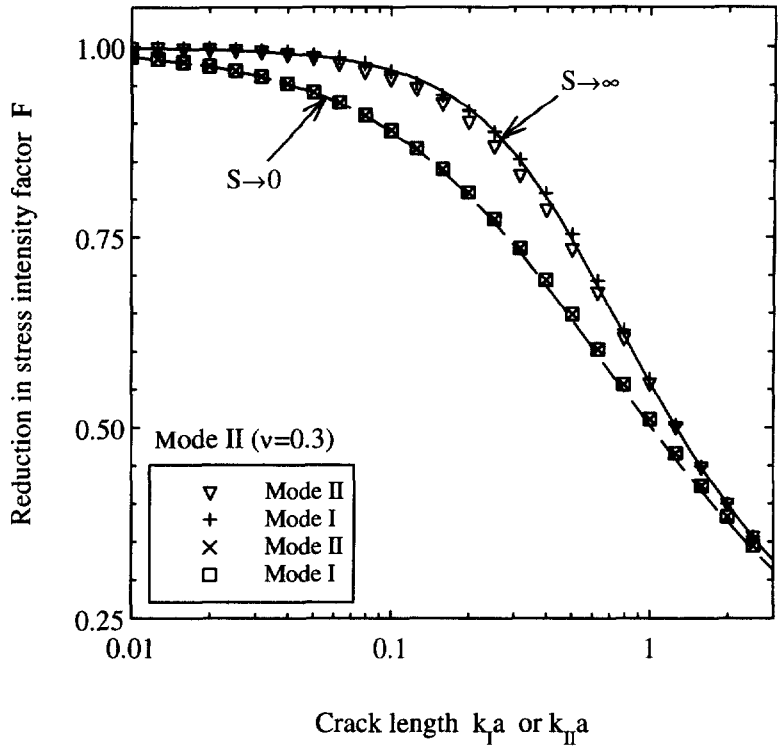

Fig. 9. Comparison between mode I and mode II stress intensity factors. Symbols: exact solution of the integral equation (mode I and mode II); solid curve: eqn (95) with B = 0.1. Dashed curve: eqn (94).

mode II stress intensity factors, as shown in Fig. 9. These results reveal that, for a given stiffness ratio, the repair efficiency can be completely characterised by two scaling parameters: shear transfer length and spring constant, both of which depend on loading mode and the Poisson's ratio.

The crack bridging model of reinforcement by distributed springs has been extensively used in a number of contexts ranging from crack patching to composite fracture. The present results revealed that, however, there is a significant limitation of the crack bridging model in capturing the asymptotic behaviour in the short crack limit, especially in the context of crack patching. In idealising the reinforcement as springs distributed over the crack faces, the load transfer from the cracked plate to the reinforcement has effectively been assumed to occur over zero distance, whereas in reality this transfer occurs over a finite region surrounding the crack. As shown in Fig. 9, this simplification would result in a non-conservative estimate of the repair efficiency. By the same token, the existing models for analysing fibre bridging of cracks in composites (Marshall, Cox, and Evans, 1985; Nemat-Nasser and Hori, 1987; Budiansky and Amazigo, 1989; Cox and Rose, 1994) may also lead to non-conservative predictions, and hence need to be modified to accommodate the gradual stress transfer between the matrix and the fibres arising from fibre pull-out.

To summarise, the following conclusions can be drawn from the present work:

1. An analytical solution has been obtained for the stress intensity factor of a crack under mode II after being repaired by a bonded reinforcement.
2. The mode II stress intensity factor asymptotes to a limiting value as the crack length increases to infinity; a closed-form solution has been obtained for this asymptotic value.
3. In the case of an isotropic plate reinforced by an isotropic patch, the asymptotic value of the mode II stress intensity is considerably higher than that in mode I, for the same nominal applied stress.

4. The asymptotic stress intensity factor for mode II cracks depend strongly on the shear moduli of the crack plate and the reinforcement.
5. Anisotropic reinforcements with low shear moduli are not suitable for repairing cracks which are subjected to shear loading, although they may be most efficient in reducing the stress intensity factor under mode I loading.
6. Two important scaling parameters have been identified which characterise the stress intensity factor of a patched crack under mode I and mode II loading.

REFERENCES

Baker, A. A. (1993) Repair efficiency in fatigue-cracked aluminium components reinforced with Boron/Epoxy patches. *Fatigue Fract. Engng Mater. Struct.* **16**(7), 753–765.

Baker, A. A. (1995) Bonded composite repair of metallic aircraft components—overview of Australia Activities. In *Composite Repair of Military Aircraft Structures*. AGARD-CP-550.

Baker, A. A. and Jones, R. (ed.) (1988) *Bonded Repair of Aircraft Structures*. Martinus Nijhoff Publishers.

Budiansky, B. and Amazigo, J. C. (1989) Toughening by aligned, frictionally constrained fibres. *Journal of Mechanics and Physics of Solids* **37**(1), 93–109.

Ching-Hwei Chue, Li-Chung Chang and Jang-Shing Tsai (1994) Bonded repair of a plate with inclined central crack under biaxial loading. *Composite Structures* **28**, 39–45.

Cox, B. N. and Rose, L. R. F. (1994) Time-or-cycle-dependent crack bridging. *Mechanics of Materials* **19**, 39–57.

Erdelyi, A. (1954) *Table of Integral Transforms*. Vol. 1. McGraw-Hill Book Company, Inc., New York.

Erdogan, F. and Arin, K. (1972) A sandwich plate with a part-through and debonding crack. *Engineering Fracture Mechanics* **4**, 449–458.

Keer, L. M., Lin, C. T. and Mura, T. (1976) Fracture analysis of adhesively bonded sheets. *Journal of Applied Mechanics* **98**(4), 652–656.

Marshall, D. B., Cox, B. N. and Evans, A. G. (1985) The mechanics of matrix cracking in brittle-matrix fibre composites. *Acta. Metall.* **33**(11), 2013–2021.

McCartney, L. N. (1992) Theory of a stress transfer in a 0°–90°–0° cross-ply laminate containing a parallel array of transverse cracks. *Journal of Mechanics and Physics of Solids* **40**(1), 27–68.

Nemat-Nasser, S. and Hori, M. (1987) Toughening by partial or fully bridging of cracks in ceramics and fibre reinforced composites. *Mechanics of Materials* **6**, 475–484.

Press, W. H., Teukolsky, S. A., Vetterling, W. T. and Flannery, B. P. (1992) *Numerical Recipes in Fortran*. Cambridge University Press, Cambridge.

Ratwani, M. M. (1979) Cracked, adhesively bonded laminated structures. *AIAA Journal* **17**(9), 988–994.

Rose, L. R. F. (1981) An application of the inclusion analogy for bonded reinforcements. *International Journal of Solids and Structures* **17**, 827–838.

Rose, L. R. F. (1982) A cracked plate repaired by bonded reinforcements. *International Journal of Fracture* **18**(2), 135–144.

Rose, L. R. F. (1987) Crack reinforcement by distributed springs. *Journal of Mechanics and Physics of Solids* **35**(4), 383–405.

Rose, L. R. F. (1988) Theoretical analysis of crack patching. In *Bonded Repair of Aircraft Structures*, ed. A. A. Baker and R. Jones, pp. 77–105. Martinus Nijhoff Publishers.

Sneddon, I. N. and Lowengrub, M. (1969) *Crack Problems in the Classical Theory of Elasticity*. John Wiley and Sons, Inc., New York.

Wang, C. H. and Brown, M. W. (1993) A path-independent parameter for fatigue under proportional and non-proportional loading. *Fatigue Fract. Engng Mater. Struct.* **16**, 1285–1298.

Wang, C. H. and Brown, M. W. (1996) Life prediction techniques for variable amplitude multiaxial fatigue—part 1: theories. *Journal of Engineering Materials and Technologies* **118**, 367–370.

Wang, C. H., Rose, L. R. F. and Callinan, R. (1997) Analysis of out-of-plane bending of one-sided repair. *International Journal of Solids and Structures* (in press).

APPENDIX A: STRESS DISTRIBUTION IN THE REINFORCED REGION

Determination of the stress distribution in a reinforced region involves two stages: the stress concentration caused by the increased stiffness of the reinforced region, and the stress sharing between the plate and the patch. These two aspects are frequently coupled, giving rise to a rather complex stress analysis problem with irregular boundaries. Solutions of the stresses in a reinforced region are available only for certain simple shapes and load distributions. For instance, in the case of uniform biaxial tension at infinity, Rose (1981) presented an analytical treatment for an elliptical reinforcement, which involved solving two simultaneous linear equations.

However, in the case when the stress concentration can be ignored, a simple solution of the stress distribution in a reinforced plate that is subjected to uniform biaxial stresses at infinity can be readily determined. For the geometry shown in Fig. 1,

$$\sigma_{xx} = \sigma^{\infty}_{xx}, \quad \sigma_{yy} = \sigma^{\infty}_{yy}, \quad \tau_{xy} = \tau^{\infty}_{xy}. \tag{A1}$$

It is assumed that both the base plate and the reinforcement are isotropic and homogeneous, and the bond allows no relative displacement between the plate and the reinforcement, i.e. the strains in the base plate are equal to the strains in the reinforcement,

$$\varepsilon_{\alpha\beta}^{P} = \varepsilon_{\alpha\beta}^{R}, \tag{A2}$$

where and in the following superscripts P and R denote the quantities pertaining to the base plate and the reinforcement, respectively. The subscripts α and β range over x and y.

According to Hooke's law for plane stress condition,

$$\sigma_{xx}^{P,R} = \frac{E_{P,R}}{1-\nu_{P,R}^2}(\varepsilon_{xx} + \nu_{P,R}\varepsilon_{yy}), \tag{A3a}$$

$$\sigma_{yy}^{P,R} = \frac{E_{P,R}}{1-\nu_{P,R}^2}(\varepsilon_{yy} + \nu_{P,R}\varepsilon_{xx}), \tag{A3b}$$

$$\tau_{xy}^{P,R} = \frac{E_{P,R}}{2(1+\nu_{P,R})}\gamma_{xy}. \tag{A3c}$$

Now suppose that stresses in the plate and the reinforcement are uniform, the equations of equilibrium may be written as follows, ignoring stress concentration due to reinforcement,

$$\sigma_{xx}^{P} t_P + \sigma_{xx}^{R} t_R = \sigma_{xx}^{\infty} t_P, \tag{A4a}$$

$$\sigma_{yy}^{P} t_P + \sigma_{yy}^{R} t_R = \sigma_{yy}^{\infty} t_P, \tag{A4b}$$

$$\tau_{xy}^{P} t_P + \tau_{xy}^{R} t_R = \tau_{xy}^{\infty} t_P. \tag{A4c}$$

From equations (A3) and (A4), the strains can be readily solved,

$$\varepsilon_{xx} = \frac{\sigma_{xx}^{\infty} t_P \left(\frac{E_P t_P}{1-\nu_P^2} + \frac{E_R t_R}{1-\nu_R^2}\right) - \sigma_{yy}^{\infty} t_P \left(\frac{E_P t_P \nu_P}{1-\nu_P^2} + \frac{E_R t_R \nu_R}{1-\nu_R^2}\right)}{\left[\frac{E_P t_P}{1-\nu_P^2} + \frac{E_R t_R}{1-\nu_R^2}\right]^2 - \left[\frac{E_P t_P \nu_P}{1-\nu_P^2} + \frac{E_R t_R \nu_R}{1-\nu_R^2}\right]^2}, \tag{A5a}$$

$$\varepsilon_{yy} = \frac{\sigma_{xx}^{\infty} t_P \left(\frac{E_P t_P \nu_P}{1-\nu_P^2} + \frac{E_R t_R \nu_R}{1-\nu_R^2}\right) - \sigma_{yy}^{\infty} t_P \left(\frac{E_P t_P}{1-\nu_P^2} + \frac{E_R t_R}{1-\nu_R^2}\right)}{\left[\frac{E_P t_P \nu_P}{1-\nu_P^2} + \frac{E_R t_R \nu_R}{1-\nu_R^2}\right]^2 - \left[\frac{E_P t_P}{1-\nu_P^2} + \frac{E_R t_R}{1-\nu_R^2}\right]^2}, \tag{A5b}$$

$$\gamma_{xy} = \frac{\tau_{xy}^{\infty} t_P}{\frac{E_P t_P}{2(1+\nu_P)} + \frac{E_R t_R}{2(1+\nu_R)}}. \tag{A5c}$$

The stresses in either the plate or the reinforcement are given by eqns (A3). In particular, one special case of importance here is that the plate and the reinforcement have the same Poisson's ratio (i.e. $\nu_P = \nu_R = \nu$). The solutions in this case can be considerably simplified,

$$\varepsilon_{xx} = \frac{(\sigma_{xx}^{\infty} - \nu\sigma_{yy}^{\infty}) t_P}{E_P t_P + E_R t_R}, \tag{A6a}$$

$$\varepsilon_{yy} = \frac{(\sigma_{yy}^{\infty} - \nu\sigma_{xx}^{\infty}) t_P}{E_P t_P + E_R t_R}, \tag{A6b}$$

$$\gamma_{xy} = \frac{2(1+\nu)\tau_{xy}^{\infty} t_P}{E_R t_R + E_P t_P}. \tag{A6c}$$

Consequently,

$$\sigma_{xx}^{P} = \frac{1}{1+S}\sigma_{xx}^{\infty}, \tag{A7a}$$

$$\sigma_{yy}^{P} = \frac{1}{1+S}\sigma_{yy}^{\infty}, \tag{A7b}$$

$$\tau_{xy}^{P} = \frac{1}{1+S}\tau_{xy}^{\infty}, \tag{A7c}$$

where $S = E_R t_R / E_P t_P$ denotes the stiffness ratio.

APPENDIX B: EXPRESSIONS FOR MODE I

The following equations represent the mode I analogous of the results given by eqns (36), (42), (43) and (44) for mode II.

$$F_1(\xi) = \frac{(2\xi^2 + \lambda^2)^2 - 4\lambda_1\lambda_2\xi^2}{(1+\nu)\lambda_2\xi}, \tag{B1}$$

$$L_1(t,r) = \int_0^\infty (F_1(\xi) - \xi) J_0(\xi t) J_0(\xi r)\, \mathrm{d}\xi, \tag{B2}$$

$$\Phi(r) + \frac{S}{1+S} r \int_0^a L_1(t,r)\Phi(t)\, \mathrm{d}t = -\frac{\sigma_0 r}{(1+\nu)\mu_P}, \tag{B3}$$

$$K_1 = -(1+\nu)\mu_P\sqrt{\pi}\frac{\Phi(a)}{\sqrt{a}}. \tag{B4}$$